RESEARCH ARTICLE | MARCH 09 2018

Lipid diffusion in the distal and proximal leaflets of supported lipid bilayer membranes studied by single particle tracking

Special Collection: Single Molecule Biophysics

Rafael L. Schoch ; Itay Barel ; Frank L. H. Brown; Gilad Haran

J. Chem. Phys. 148, 123333 (2018)
https://doi.org/10.1063/1.5010341
CHORUS

Lipid diffusion in the distal and proximal leaflets of supported lipid bilayer membranes studied by single particle tracking

Rafael L. Schoch,[1] Itay Barel,[2] Frank L. H. Brown,[2] and Gilad Haran[1]
[1]*Department of Chemical and Biological Physics, Weizmann Institute of Science, P.O. Box 26, Rehovot 7610001, Israel*
[2]*Department of Chemistry and Biochemistry and Department of Physics, University of California, Santa Barbara, Santa Barbara, California 93106, USA*

(Received 24 October 2017; accepted 9 February 2018; published online 9 March 2018)

Supported lipid bilayers (SLBs) have been studied extensively as simple but powerful models for cellular membranes. Yet, potential differences in the dynamics of the two leaflets of a SLB remain poorly understood. Here, using single particle tracking, we obtain a detailed picture of bilayer dynamics. We observe two clearly separate diffusing populations, fast and slow, that we associate with motion in the distal and proximal leaflets of the SLB, respectively, based on fluorescence quenching experiments. We estimate diffusion coefficients using standard techniques as well as a new method based on the blur of images due to motion. Fitting the observed diffusion coefficients to a two-leaflet membrane hydrodynamic model allows for the simultaneous determination of the intermonolayer friction coefficient and the substrate-membrane friction coefficient, without any prior assumptions on the strengths of the relevant interactions. Remarkably, our calculations suggest that the viscosity of the interfacial water confined between the membrane and the substrate is elevated by $\sim 10^4$ as compared to bulk water. Using hidden Markov model analysis, we then obtain insight into the transbilayer movement of lipids. We find that lipid flip-flop dynamics are very fast, with half times in the range of seconds. Importantly, we find little evidence for membrane defect mediated lipid flip-flop for SLBs at temperatures well above the solid-to-liquid transition, though defects seem to be involved when the SLBs are cooled down. Our work thus shows that the combination of single particle tracking and advanced hydrodynamic modeling provides a powerful means to obtain insight into membrane dynamics. *Published by AIP Publishing.* https://doi.org/10.1063/1.5010341

INTRODUCTION

Supported lipid bilayers (SLBs) are commonly used as simplified mimics of cellular membranes in order to gain insight into basic membrane dynamics and function.[1–7] For instance, the thermodynamics of phase behavior and lipid domain formation is largely preserved in SLBs and can be investigated by various surface-specific techniques.[8–15] While lipids are considered free to diffuse in the fluid two-dimensional space formed by the SLB, it is well known that substrate proximity leads to a reduction in lipid mobility relative to free standing membranes.[4,16,17] Depending on the preparation technique, lipid probe, and substrate type, either uniform[11,16,18–21] or bimodal[11,21–26] lipid diffusivity has been reported in the fluid phase of SLBs. Though it has been reasoned that the bimodal diffusion arises from different dynamics of the proximal and distal leaflets of the membrane,[11,21,22,24] this proposal has only been clearly validated for membranes on silica beads.[22] Alternatively, bilayer heterogeneity, defect structures, probe clustering, probe immobilization, and probe orientation have been suggested to cause the disparities in diffusivity.[4,11,15,17,25–27]

In the popular description for membranes supported by a planar substrate, due to the work of Evans and Sackmann,[18,28] it is assumed that momentum transfer in the membrane is dominated by the presence of the substrate. The amount of frictional coupling between the membrane and the substrate depends on the thickness and viscosity of the water layer separating the two.[18,28] However, the hydrodynamic model of Evans and Sackmann treats the membrane as a single sheet, ignoring its dual leaflet structure. In the case of strong substrate-membrane coupling, partial decoupling may take place between the two leaflets of the membrane, which may be behind the appearance of two diffusion coefficients, as mentioned above.[21,24,29] Such a decoupling was observed in studies of the solid-to-liquid phase transition of the proximal and distal leaflets of SLBs.[8–10] Preparation of an asymmetric SLB can be used to shed light on this phenomenon. However, this approach is only meaningful if the bilayer does not equalize its composition within the experimental preparation times.[14,24] Indeed, lipid flip-flop, i.e., the transbilayer movement of lipids, is considered to be faster for SLBs as compared to free standing membranes.[30–34] Potential explanations for the high flip-flop rates in SLBs include membrane defects remaining from the preparation process,[35] as well as surface induced acyl chain disorder.[33] Experiments on SLBs in the fluid phase[31,32] suggested flip-flop half times of the order of seconds.

Single-particle tracking (SPT) of membrane bound probes is extensively used to investigate the dynamics of lipid molecules or membrane-embedded proteins by direct observation at high temporal resolution and nanometer-scale precision.[36] In contrast to ensemble-averaged measurements, SPT

allows detecting subpopulations and rare dynamic events.[37,38] This method is capable of revealing the nanoscale dynamics of either protein or lipid probes in the natural context of the cell plasma membrane,[38–42] as well as in SLBs, where it has been used to reveal virus-membrane binding,[6] switching between diffusive modes of membrane inserting peptides,[3] or the influence of membrane curvature on lipid dynamics.[5]

Here, we apply dual-color SPT to simultaneously track the motion of two labeled lipids within 1,2-dioleoyl-*sn*-glycero-3-phosphocholine (DOPC) and egg L-α-phosphatidylcholine (EPC) membranes in the fluid phase. We also introduce a novel method to estimate diffusion coefficients from individual frame images, based on the blur of the shapes of particles due to their motion. A Hidden Markov Model (HMM) analysis[3,43] allows us to distinguish between different diffusive modes and to estimate their transitional dynamics. Iodine quenching experiments are used in order to associate slow and fast diffusing populations with the proximal and distal leaflets of the SLB, respectively. The transitions of probes between the two diffusive modes are therefore attributed to the flip-flop of lipids. Theoretical analysis based on the "Regularized Stokeslets" method, which takes into account the dual-leaflet nature of the bilayer,[44] further allows us to obtain estimates for the membrane-substrate and inter-leaflet friction coefficients.

MATERIALS AND METHODS

SLB preparation and imaging

Flow cells were prepared using two microscope cover glasses (24 × 50 mm and 18 × 18 mm, No1, Marienfeld, Germany) that were first etched in 10% HF (hydrofluoric acid 40%, Merck, Germany) for 40 s while sonicating. The slides were then rinsed with Milli-Q H_20, dried in a N_2 stream, and glued together using two thin Parafilm (Bemis Company, USA) stripes followed by curing in an oven for 15 min at 115 °C. For the preparation of SLBs, 10 mg/ml Egg L-α-phosphatidylcholine (EPC, Avanti Polar Lipids Inc., USA) or 1,2-dioleoyl-sn-glycero-3-phosphocholine (DOPC, Avanti Polar Lipids, Inc., USA) were dissolved in tert-butanol (Sigma, USA). Atto550 headgroup-labeled 1,2-dimyristoyl-sn-glycero-3-phosphoethanolamine (Atto550-DMPE, ATTO-TEC, Germany) as well as Atto647N-DMPE (ATTO-TEC, Germany) were dissolved in chloroform (Bio-Lab ltd., Israel). The labeled lipids were then separately added to the lipid solution to obtain a $\sim 5 \times 10^{-5}$ mol % solution of labeled lipids. The lipid solutions were aliquoted, lyophilized, and stored at −20 °C. One aliquot of each lipid solution was then re-suspended to 10 mg/ml in the experimental buffer (50 mM TRIS, 100 mM NaCl, pH 7.5), extruded together through a 0.1 μm filter (Whatman Anotop, GE Healthcare, USA) to create unilamellar vesicles[45] and stored at 4 °C. The flow cells were rinsed four times with 200 μl of the experimental buffer and then loaded and incubated with 50 μl of the vesicle solution for 5 min. The flow cells were rinsed again four times with 200 μl of the experimental buffer solution and directly used. In quenching experiments, the flow cells were rinsed two times with the experimental buffer solution and then four times with an iodide solution (50 mM TRIS, 100 mM KI, 0.1 mM $Na_2S_2O_3$, pH 7.5). SLBs were imaged using a dual color total internal reflection fluorescence (TIRF) microscope equipped with an electron-multiplying charge-coupled device (EMCCD) camera (Andor iXon 897), at a frame rate of 128.87 Hz. For a complete description of the TIRF setup, as well as ensemble fluorescence spectroscopy, please see Secs. S1 and S2 of the supplementary material.

SPT analysis algorithm

The detection and tracking of particles was implemented in Matlab (MathWorks, USA). In brief (see Secs. S3–S6 of the supplementary material for more details), the extraction of spots was performed using a B3-spline version of the à trous wavelet transform.[46] The detected spots were then fitted using a symmetric Gaussian model point spread function (PSF), with the expected photon count E_n at pixel n given by

$$E_n = b^2 + I_{ph} \cdot \exp\left(-\frac{(x_n - \mu_x)^2}{2\sigma_a^2} - \frac{\left(y_n - \mu_y\right)^2}{2\sigma_a^2}\right), \quad (1)$$

where b^2 is the background level, I_{ph} is the amplitude, μ_x and μ_y are the subpixel positions of a particle, σ_a is the Gaussian standard deviation, and x_n, y_n are the pixel positions. For iterative fitting of Eq. (1), we used a maximum likelihood estimation (MLE) method for Poisson distributed photon counting events,[47] based on a modified Levenberg-Marquardt (LM) algorithm.[48]

For particle tracking and linking between camera frames, we used an approach based on the linear assignment problem (LAP),[49] with modifications to the cost matrix for particle assignment. After linking the particles, HMM analysis[3,43] was applied to the full set of trajectories with a minimal length of five steps. The fast and slow diffusion states in each trajectory were then assigned by determining the single best state sequence, using the Viterbi algorithm.[3,43] Following state assignment, we then used covariance-based estimation (CVE) analysis[50] to extract diffusion coefficients from individual trajectories. For each SLB type, a total of 60 000–110 000 trajectories were analyzed for Atto550-DMPE and 30 000–45 000 for Atto647N-DMPE.

The SPT algorithm was carefully evaluated by using simulated EMCCD recordings that mimic the experimentally obtained data, including a full statistical treatment of the electron multiplication gain, noise contributions, and sub-frame molecular motion. For comparing flip-flop positions of the two differently labeled lipids, image registration was applied using a linear system of equations[39] solved for the positions of microbeads, which were recorded before and after each SPT experiment, and the results were used to transform the positions of the lipid probes.

Motion blur analysis

A motion blur analysis method was developed to obtain diffusion coefficients of the fast moving particles from the shapes of particle images in individual frames. To this end, we superimposed images of single particles (after assigning their trajectories to either the fast or slow state) by co-aligning them with respect to their subpixel position $(\hat{\mu}_x, \hat{\mu}_y)$ obtained using Eq. (1). Co-alignment was achieved by translating images in

frequency space using the fast Fourier transform algorithm *fft2* from Matlab. As we co-aligned the particle images with respect to their estimated subpixel positions $(\hat{\mu}_x, \hat{\mu}_y)$, this procedure introduced the dynamic localization uncertainty $\sigma_i(D_i)$ as an error in co-alignment, where the index i specifies the state, either "fast" or "slow." Thus, for example, $\hat{\mu}_x = \tilde{\mu}_x + \chi_i$ where $\chi_i \sim N(0, \sigma_i)$ is normally distributed with a zero mean and a standard deviation $\sigma_i(D_i)$, and $\tilde{\mu}_x$ denotes the true particle position. An analogous expression is relevant for y. In our analysis, we defined the dynamic localization uncertainty for a moving probe $\sigma_i^2(D_i)$ in state i, including motion blur, as follows:

$$\sigma_i^2(D_i) \approx \sigma_0^2 \cdot \left(1 + D_i \Delta t_{ex}/3 s_{0,th}^2\right) \cdot N_{corr,i}, \tag{2}$$

where the factor $D_i \Delta t_{ex}/3$ is the variance in trajectory positions due to diffusion[50,51] (i.e., causing motion blur), $\Delta t_{ex} = 7.49$ ms is the exposure time of the camera, $s_{0,th} = 0.21\lambda/NA$ is the theoretical diffraction limited PSF width[52] as a function of wavelength λ and numerical aperture NA, and $N_{corr,i}$ is correcting for the number of emitted photons. Eq. (2) is based on the approximation[52] $\sigma_i^2 \approx s_i^2/N$ in combination with[50,51] $s_i^2 \approx s_{0,th}^2 + D_i \Delta t_{ex}/3$. Here, the static localization uncertainty $\sigma_0(D = 0)$ was approximated by the theoretical localization precision σ_{lp}, where σ_{lp} was calculated as explained in Ref. 47 from MLE of the slow diffusing probes, i.e., $\sigma_0^2 \approx \langle \sigma_{lp,slow} \rangle^2$. Further, $\sigma_i^2(D_i)$ was corrected for the average photon emission $\langle N_i \rangle$ of an individual state using $N_{corr,i} = \langle N_{slow} \rangle / \langle N_i \rangle$, where $\langle N_{slow} \rangle$ is the average photon emission of the slow particles.

The superimages resulting from the superposition of co-aligned particle images were then least-squares fitted with the Gaussian PSF of Eq. (1) and related to the diffusion coefficient D_i using[50]

$$\sigma_{a,i}^2(D_i) = s_0^2 + a^2/12 + D_i \Delta t_{ex}/3 + \sigma_i^2(D_i), \tag{3}$$

where $s_a^2 = s_0^2 + a^2/12$ is the width of the diffraction limited Gaussian PSF s_0, corrected for the pixel size[47] ($a = 107$ nm), and Δt_{ex} is the camera exposure time per frame.

Here it is important to have an accurate measure of the diffraction limited PSF width s_0^2. To obtain s_0^2 experimentally for our setup, we used $\sigma_{a,slow}^2$ (i.e., for state $i =$ "*slow*") from the superimage of the slow moving probes to solve Eq. (3) for s_0^2 using D_{slow} from CVE analysis and $\sigma_{slow}^2(D_{slow}) \approx \langle \sigma_{lp,slow} \rangle^2$ from the same experiment. The latter is a valid approximation for slow moving probes, i.e., if $D\Delta t_{ex} < s_0^2$, as can be seen from Eq. (2). To finally obtain $D_{fast}(\sigma_a^2)$ (i.e., for state $i =$ "*fast*") from the superimage of the fast particles, we solved Eq. (3) using the experimental s_0^2 as well as $\sigma_{fast}^2(D_{fast})$ obtained from Eq. (2).

EXPERIMENTAL RESULTS

Slow and fast diffusion of lipids in SLBs

We recorded movies of fluorescent lipids diffusing in lipid bilayers supported on a microscope glass slide. Diffusive trajectories were created by detecting spots in individual frames and linking them in consecutive frames of the movies, as discussed in the section titled Materials and methods. They were then analyzed using a two-state HMM model in combination with the Viterbi algorithm.[3,43] This enabled us to assign the sequence of states for individual trajectories, and by selecting the trajectories associated with each state, we obtained two well-separated populations of slow and fast diffusing particles. In Figs. 1(a) and 1(b), we show sample trajectories of slow and fast diffusing Atto647N-DMPE lipids in DOPC SLBs. Distributions of diffusion coefficients D of single trajectories of the two types of lipids (i.e., for Atto550-DMPE and Atto647N-DMPE) obtained using CVE analysis[50] are shown in Figs. 1(c) and 1(d), respectively. D values associated with the fast state are shown in green whereas those associated with the slow state are shown in blue. In the histograms, each count represents a single trajectory. We note however that due to the way the experiment and analysis were conducted, the populations of the slow and fast diffusing molecules are not representative of their true state populations under equilibrium. As we measured with relatively high laser intensities, we reached a steady state where molecules within the field of view are photobleached and mainly fast particles are entering the image before they also photobleach. Further, the fast trajectories have fewer steps on average than the slow trajectories (i.e., for Atto647N-DMPE 14 fast steps vs. 37 slow steps). The values of the diffusion coefficients D_{fast} and D_{slow} for a single sample were obtained from fitting a Gaussian distribution to each population in the distributions. Table I summarizes the diffusion coefficients obtained for EPC and DOPC SLBs as averages over several samples.

All samples consistently revealed slow and fast diffusing populations of lipid probes. The values reported in Table I are in good agreement with diffusion coefficients reported before for similar bilayer systems based on either SPT[23,25] or fluorescence correlation spectroscopy (FCS),[20] though no slow population was identified by the latter method. We emphasize that the localization uncertainty is embedded into CVE analysis, and thus the values obtained are free of this contribution. When measuring at 10 °C, the diffusion slows down to about half the values measured at RT for the DOPC membranes. As the movies were recorded in dual color, this allowed us to directly compare the diffusion of the differently labeled lipids. We noticed that Atto550-DMPE lipids are diffusing slightly faster than Atto647N-DMPE lipids as consistently revealed under each experimental condition.

Motion blur analysis

In addition to the trajectory-based analysis discussed above, we also considered extracting diffusion coefficients from individual frame images. The average width σ_a^2 of a particle image, according to Eq. (3), depends on the diffraction limited PSF width s_0^2 and the diffusion coefficient D, which causes a variance $D\Delta t_{ex}/3$ in the particle position.[51] For a finite exposure time Δt_{ex} of the camera, this leads to larger particle images, a phenomenon known as motion blur. However, as shown in Fig. 2(a), the scattering in the estimates $\hat{\sigma}_a$ from Eq. (1) is too large to infer diffusional properties from single probe images. Therefore, in order to obtain average properties, we superimposed images of single particles by co-aligning them with respect to their subpixel localization

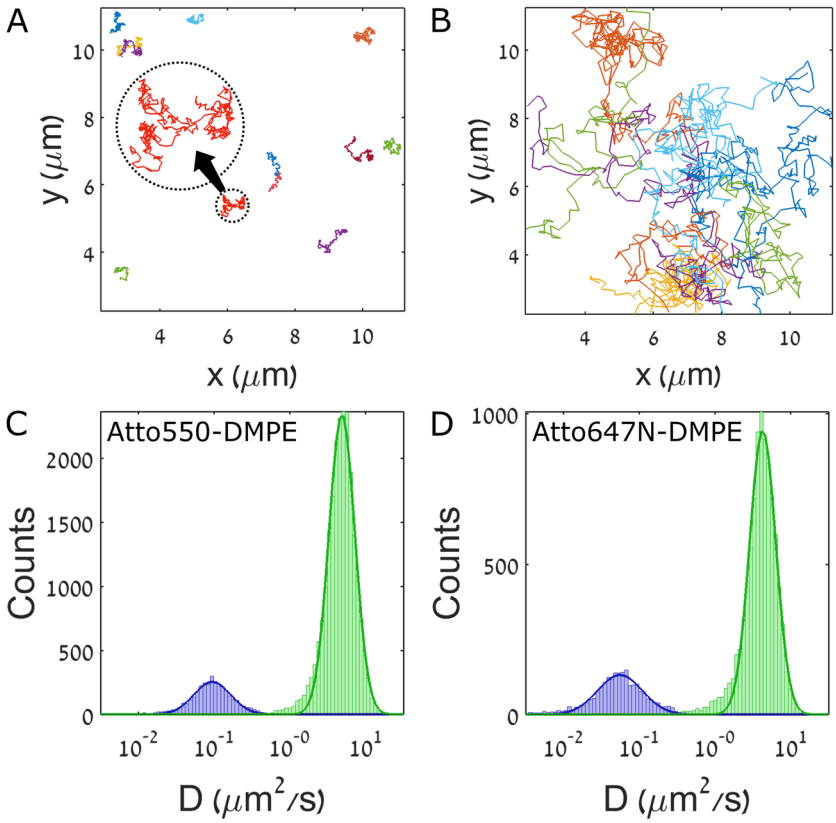

FIG. 1. Slow and fast diffusion of lipids in DOPC SLBs. (a) Trajectories of slow moving lipids. (b) Trajectories of fast moving lipids. (c) Distribution of D values of Atto550-DMPE obtained from CVE analysis of single trajectories, revealing a fast population (green) and a slow population (blue). (d) Same as in (c) for Atto647N-DMPE.

position $(\hat{\mu}_x, \hat{\mu}_y)$. Contour plots of summed particle images are shown in Figs. 2(b) and 2(c) for slow and fast moving populations of Atto647N-DMPE in a DOPC SLB. The images were taken from the same trajectories as for the distributions shown in Fig. 1(d). As can be seen, the resulting superimages are highly symmetric, whereas the individual particle images are asymmetric due to stochastic Brownian motion and photon statistics [see insets in Fig. 2(a)]. We extracted the width $\sigma^2_{a,i}(D_i)$ of the superimages of state i = "*fast*" or "*slow*," by least squares fitting the Gaussian model PSF Eq. (1). As we did not know the exact width s_0^2 of the diffraction limited PSF, we first used the slow superimage to estimate s_0^2, given $D_{slow,CVE}$ from CVE analysis and $\langle\sigma_{lp,slow}\rangle^2$ from the same experiment, and subsequently used the fast superimage to estimate $D_{fast}(\sigma_a^2)$ using Eq. (3). For more details, see the section titled Materials and methods. We obtained $D_{fast}(\sigma_a^2)$ = 4.31 μm^2/s from the superimage of the fast diffusing particles. This value is in good agreement with the diffusion coefficient $D_{fast,CVE}$ = 4.22 ± 0.02 μm^2/s obtained from CVE analysis. While the influence of localization precision is minor here, most critical to this method is to know s_0^2 of the imaging system, and if available (we have deduced it from the slow particles here) it can be used to obtain good estimates for the diffusion of particles simply from the shape of the average blurred particle images.

While in Figs. 2(b) and 2(c) we superimposed thousands of particle images, we also tested whether motion blur analysis can be applied using a smaller number of images. In Fig. 2(d), we show the performance of the method as a function of the number of images superimposed. The figure shows that using only single images to obtain σ_a^2 and thus $D(\sigma_a^2)$ leads to a serious overestimation of the diffusion coefficient $D_{fast}(\sigma_a^2)$ when compared to $D_{fast,CVE}$. Further, the variance of the estimates is huge in this case. However, the more particles are superimposed, the better the estimate $D_{fast}(\sigma_a^2)$ gets. With a signal to noise ratio of ~3.5, good estimates are obtained from superimposing at least 100 probe images. We additionally show a value of $D_{fast}\left(\left\langle\hat{\sigma}_a^2\right\rangle\right)$ that was obtained by averaging the MLE

TABLE I. Diffusion coefficients of different lipid-dye combinations. Single-particle trajectories were measured either at room temperature (RT) or 10 °C, and CVE analysis was performed as discussed in relation to Figs. 1(c) and 1(d). The values are averages over four SLB samples.

	EPC (RT) (μm^2/s)	DOPC (RT) (μm^2/s)	DOPC (10 °C) (μm^2/s)
Atto550-DMPE	D_{fast} = 4.22 ± 0.02 D_{slow} = 0.079 ± 0.002	D_{fast} = 4.89 ± 0.02 D_{slow} = 0.091 ± 0.002	D_{fast} = 2.47 ± 0.06 D_{slow} = 0.045 ± 0.001
Atto647N-DMPE	D_{fast} = 3.94 ± 0.02 D_{slow} = 0.054 ± 0.002	D_{fast} = 4.30 ± 0.02 D_{slow} = 0.052 ± 0.002	D_{fast} = 2.22 ± 0.06 D_{slow} = 0.03 ± 0.001

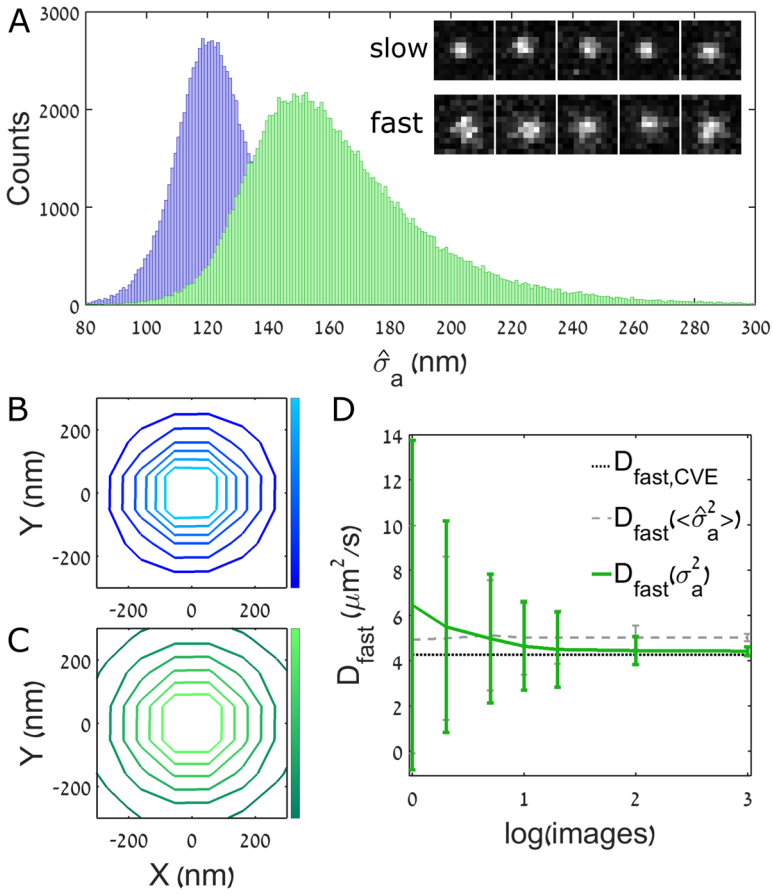

FIG. 2. Diffusion coefficients from motion blur analysis. (a) Histograms of Gaussian PSF widths $\hat{\sigma}_a$ obtained from MLE analyses of fast (green) and slow (blue) diffusing Atto647N-DMPE lipids in a DOPC SLB at RT. The insets show typical probe images for slow and fast diffusing probes. (b) Superposition of all images of the slow diffusing particles. (c) Superposition of all images of the fast diffusing particles. As can be seen in (b) and (c), the superposition of individual probe images yields highly symmetric superimages. (d) Mean diffusion coefficient $D_{fast}\left(\sigma_a^2\right)$ (solid green line) as a function of the number of images superimposed (i.e., 1, 2, 5, 10, 20, 100, 1000). The error bars show the standard deviation obtained by repeating the procedure by drawing a random set of images from the total data set. Reasonable estimates are obtained from superimposing at least 100 probe images. The results are compared to the value $D_{fast,CVE} = 4.22 \pm 0.02\,\mu\text{m}^2/\text{s}$ obtained from CVE analysis of the total data set (dotted black line). Additionally we show the estimates $D_{fast}\left(\left\langle\hat{\sigma}_a^2\right\rangle\right)$ from averaging $\left\langle\hat{\sigma}_a^2\right\rangle$ for single images without superposition (dashed gray line).

particle widths $\left\langle\hat{\sigma}_a^2\right\rangle$ without superposition. As can be seen, this measure overestimates the diffusion constant.

The novel method presented here, based on motion blur, could in principle be used to extract diffusion coefficients without the need for particle tracking. This approach is similar to spot-size analysis,[53] but uses a symmetric Gaussian function and is robust towards fitting bias and the effect of outliers due to the superposition of multiple particle images. The method can be strictly applied only to two dimensional systems, as out of focus detection leads to broadening of the image PSF.[51] It could be used to extract local diffusion coefficients relative to a reference point. Possible applications include transient interactions of lipid probes with proteins[54,55] or the transient partitioning of lipid probes into lipid rafts.[56,57]

Lipid diffusion in the proximal and distal leaflets

We hypothesized that the slow and fast populations of lipids arise from diffusion in the proximal and distal leaflets of the SLB, respectively. To verify this hypothesis, we performed fluorescence quenching experiments using molecular iodide.[58–60] First, we assessed the bulk quenching of the fluorescence of Atto647N-DMPE and Atto550-DMPE in EPC vesicles, by performing iodide concentration dependence studies using a spectrofluorometer. We compared the results to similar results obtained with the same dyes conjugated to a small protein, protein L. In Fig. 3(a), we show the relative quenching of fluorescence calculated as $1 - F/F_0$, where F_0 and F are the fluorescence emission in the absence and presence of iodide, respectively. We observed much lower quenching for dyes conjugated to DMPE in EPC vesicles (squares with solid lines), as compared to the same dyes conjugated to protein L (circles with solid lines). In the case of vesicles, to a large extent only the outer leaflet is exposed to iodide, and therefore we can assume that half of the dyes remain unquenched. However, even after taking this into account by doubling the quenching (squares with dotted lines), the quenching in the vesicles is still lower than the quenching in the protein molecules. It thus follows that both dyes are not directly exposed to the solvent and partition into the bilayer at least partially, causing a reduction in fluorescence quenching for EPC vesicles.

The finding that Atto550 and Atto647N partition into the lipid bilayer is in agreement with reported interactions of Atto647N and Atto550 with lipid bilayer membranes in bulk vesicle dialysis studies.[61] In a molecular dynamics simulation of Texas Red DHPE (TR-DHPE) in DPPC bilayers, the dye was found to reside in the upper acyl chain region of the bilayer.[62]

We then measured the amount of light emitted by single lipid probes, i.e., Atto647N-DMPE and Atto550-DMPE, in SPT experiments on SLBs in the presence and absence of iodide in the fluid above the membrane. Figure 3(b) shows the results, again presented as $1 - F/F_0$, where F_0 and F are now the average number of emitted photons per molecule in the presence of 100 mM NaCl and 100 mM KI buffer solution, respectively. When iodide was added to the SLB, the

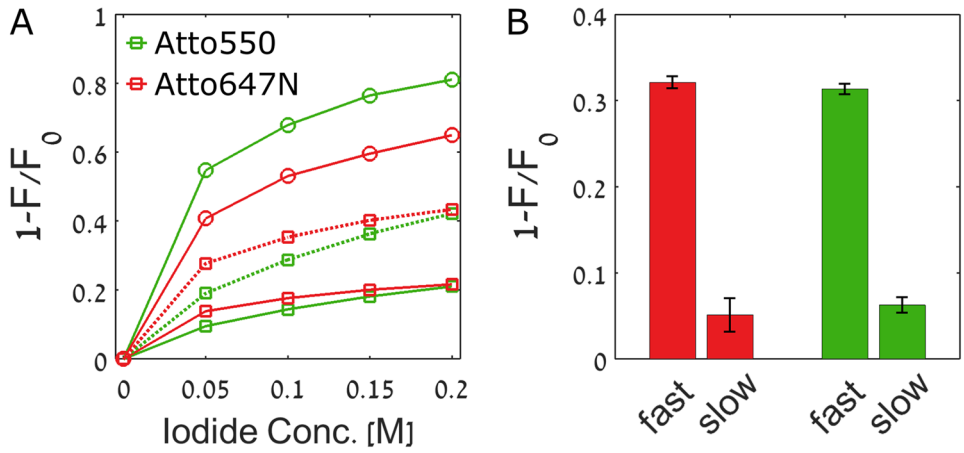

FIG. 3. Fluorescence quenching experiments. (a) Relative quenching of Atto550 (green) and Atto647N (red) when conjugated to DMPE in EPC vesicles (squares with solid lines) and when conjugated to protein L in solution (circles with solid lines). Squares with dotted lines represent doubled relative quenching, to take into account the fact that fluorophores in the lower leaflet cannot be quenched. (b) Quenching of single-particle emission due to the presence of 100 mM iodide in SPT experiments of EPC SLBs for Atto550-DMPE (green) and Atto647N-DMPE (red). It can be seen that the bulk of the quenching is associated with the fast diffusing population of Atto647N-DMPE and Atto550-DMPE. The values are averages over four SLB samples, and the error bars represent standard errors.

diffusing molecules emitted a lower number of photons. However, whereas the reduction was ~30% for the fast diffusing population of lipids, it was only ~5% for the slow diffusing population of lipids. Since iodide quenching affects the fast diffusing population much more than the slow diffusing population, we associate the fast diffusing molecules with the distal leaflet that is facing the bulk fluid and the slow diffusing molecules with the proximal leaflet facing the substrate. The quenching level of the fast lipids may in fact be somewhat underestimated, as fast lipids that are strongly quenched may not be detected anymore. The slight quenching of the slow lipids on the other hand may be due to residual leakage of iodide into the interfacial subfluid or into the lipid bilayer.[58]

Lipid flip-flop

Given that slow and fast diffusing probes are related to the proximal and distal leaflets, respectively, the state-to-state transitions we obtain from Viterbi analysis can be related to the transbilayer movement of lipids, also known as lipid flip-flop.[63] It is therefore possible to obtain the flip-flop half-times, which for Atto550-DMPE in DOPC at RT are $t_{1/2,slow} \approx 6.3 \pm 2.3$ s and $t_{1/2,fast} \approx 3.3 \pm 0.1$ s. The full set of half-times is given in Table S1 of the supplementary material. The difference between slow and fast probes suggests an asymmetric probe distribution with some preference for the proximal leaflet (see Sec. S10 of the supplementary material for a detailed discussion of this issue).

It was speculated that membrane defects in SLBs may cause shorter flip-flop half times than in vesicles.[35] To check whether this is indeed the case, we mapped the locations of transitions for both labels. To obtain a sufficient number of transitions for spatial point pattern analysis, we used rather high particle densities of ~0.04–0.1 μm^{-2}. Such high densities result in many instances where trajectories of two molecules cross each other, which may cause detection and particle assignment errors, and hence the assigned state-to-state transitions might be dominated by tracking errors. To diminish the influence of tracking errors, we therefore cropped trajectories as they got into close proximity (see Sec. S7 of the supplementary material). In simulations we found this was sufficient to remove the unwanted contribution from tracking errors and restore the correct transition probabilities using HMM (see Sec. S9 of the supplementary material). Additionally, we set the constraint that any transition in a diffusion trajectory has to be symmetrically flanked by a sequence of at least five frames, and we only considered trajectories that revealed either a single transition or none at all. This measure was taken in order to discard trajectories in which the analysis identified the highly unlikely appearance of multiple transitions and to include only well-defined transitions. Based on those constraints, we identified transition locations, as illustrated in Fig. 4(a) for a single trajectory. The sequence of particle track displacements Δr used for state assignment is shown in Fig. 4(b) for the same trajectory. The resulting transition location maps are shown in Figs. 4(c) and 4(e) for the RT and 10 °C measurements, respectively.

The analysis of the resulting spatial distribution of points was then performed using Ripley's K function,[64] which computes the normalized number of events within a circle of radius r centered on a random point of the process. The functions K_1 for Atto550-DMPE and K_2 for Atto647N-DMPE are shown in Figs. 4(d) and 4(f), as well as the cross-function K_{12}^*, describing interdependencies of the two univariate processes. If the transition points are related to specific positions in the membrane, e.g., defects, we would expect the functions K_1 and K_2 to deviate from K_{CSR}, which is Ripley's K function calculated for the case of complete spatial randomness (CSR). Similar results should hold for the function K_{12}^* if the processes are dependent. We can see from Fig. 4(d) that at RT, there is considerable agreement between the three functions and K_{CSR}, indicating spatial randomness and independence of Atto550-DMPE and Atto647N-DMPE transition locations. However, at 10 °C there seems to be weak clustering of the transition points, as seen from some deviation of the K functions from K_{CSR} in Fig. 4(f). The results suggest that while at room

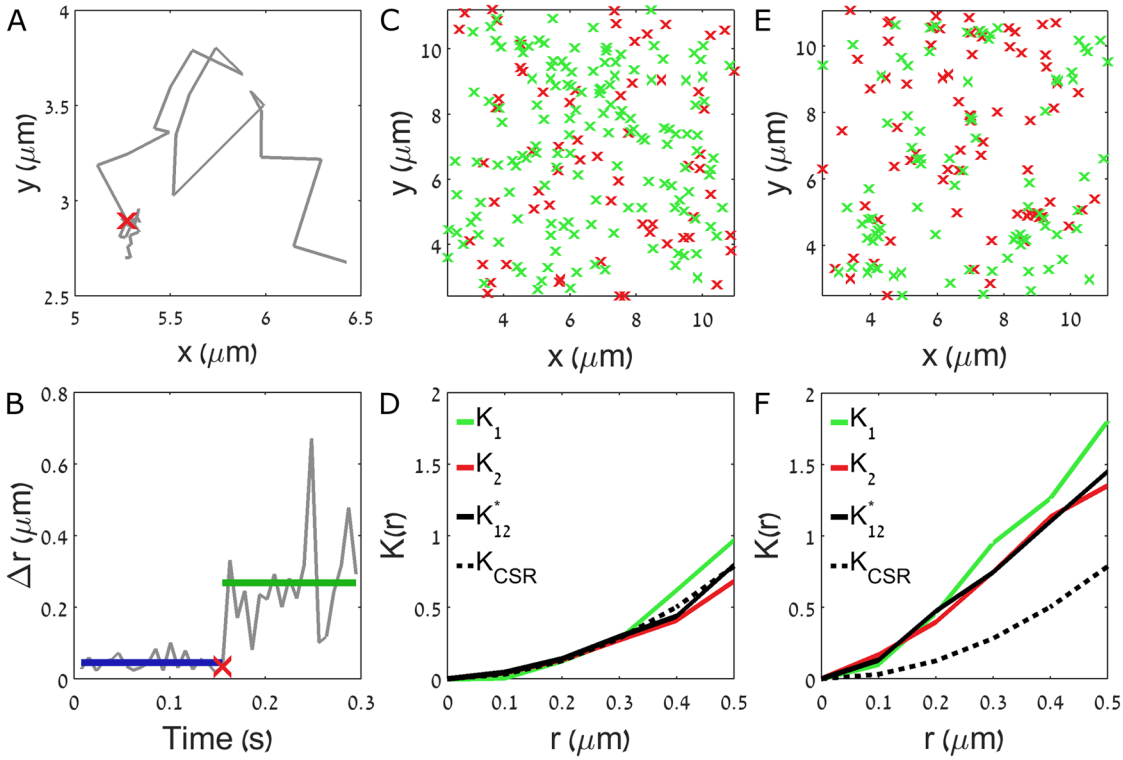

FIG. 4. Analysis of transition points in DOPC SLBs. (a) A single trajectory with the location of a state transition from slow to fast marked by a red cross. (b) Particle track displacements for the trajectory in (a) and the assigned state sequence (blue for slow steps and green for fast steps). (c) Locations of transitions for Atto550-DMPE (green) and Atto647N-DMPE (red) at RT. (e) Same as in (c) but at 10 °C. (d) Ripley's K function for Atto550-DMPE transitions (K_1, green) and for Atto647N-DMPE transitions (K_2, red), as well as the cross-type function (K^*_{12}, black solid) at RT. Also shown is the function K_{CSR} (black dotted) expected for complete spatial randomness (CSR). (f) Same as in (d) but for 10 °C.

temperature defects are unlikely to contribute to flip-flop reactions, there is some involvement of defects at 10 °C. We performed simulations to obtain more information on potential defect-based clustering, and the results suggest that at 10 °C around 40% of the flip-flop transitions belong to defects. This analysis is discussed in Sec. S11 and Fig. S5 of the supplementary material.

THEORETICAL MODELING

Numerical methods

To model the experiments, we consider a two-leaflet membrane suspended over solid support and use the Regularized Stockslets (RS) hydrodynamic numerical scheme[65,66] to predict diffusion coefficients for the labeled lipids. For a complete description of the model, we refer the reader to Ref. 44, while this section offers a brief overview of the numerical method.

We consider a modified Seifert–Langer (SL)[67] model of two coupled monolayers with a phenomenological drag between the upper (+) and lower (−) leaflets and a no-slip boundary condition for fluid flow a distance H below the bilayer [see Fig. 5(a)].[44] The Green's function T (or "membrane Oseen tensor") relates the lipid velocity field to a given applied force density

$$v_i^{\alpha}(\boldsymbol{r}) = \int d^2r' T_{ij}^{\alpha\beta}(\boldsymbol{r}-\boldsymbol{r}') f_j^{\beta}(\boldsymbol{r}'), \tag{4}$$

where the indices i,j are summed over the (x,y) Cartesian directions and the indices α,β are summed over the leaflets (+,−). The Einstein summation convention is assumed. An explicit expression for the Green's function of the two leaflet membrane system considered here is derived in Appendix A of Ref. 44 and is given by

$$T_{ij}^{\alpha\beta} = \mathcal{F}^{\alpha\beta}(\boldsymbol{q})\left(\delta_{ij} - \frac{q_i q_j}{q^2}\right), \tag{5}$$

$$\mathcal{F}^{\alpha\beta}(\boldsymbol{q}) = \frac{\left[\eta^{-\alpha}q^2 - K^{-\alpha}(q)\right]\delta^{\alpha\beta} + b_{leaflet}}{\left(q^2\eta - K^{+} + b_{leaflet}\right)\left(q^2\eta - K^{-} + b_{leaflet}\right) - b_{leaflet}^2}. \tag{6}$$

The above expressions are given in Fourier space with the convention

$$f(\boldsymbol{q}) = \int d^2r e^{-i\boldsymbol{q}\cdot\boldsymbol{r}} f(\boldsymbol{r}), \tag{7}$$

$$f(\boldsymbol{r}) = \int \frac{d^2q}{(2\pi)^2} e^{i\boldsymbol{q}\cdot\boldsymbol{r}} f(\boldsymbol{q}). \tag{8}$$

In Eq. (6), −α represents the leaflet opposite to α, $b_{leaflet}$ is the phenomenological interleaflet-friction coefficient, and η is the surface viscosity in each leaflet. The $K^{\pm}(q)$ terms account for the traction of the bounding fluid below or above each leaflet.[68] For the upper leaflet, which is adjacent to an infinite slab of fluid with viscosity η_f^+, $K^+(q) = -\eta_f^+ q$. For the bottom leaflet, which is above the solid support, $K^-(q) = -\eta_f^- q \coth(qH)$. The experiments are performed under conditions for which

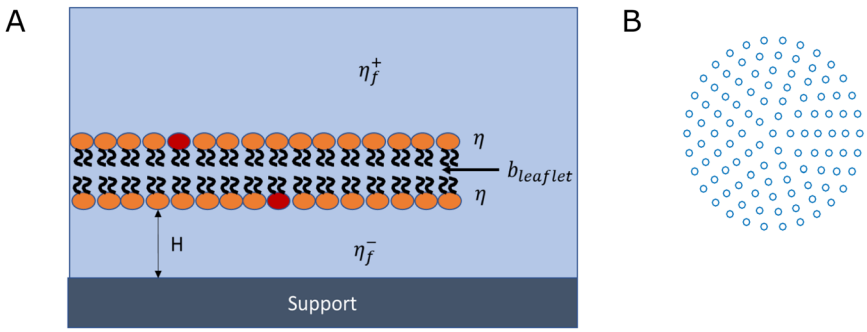

FIG. 5. Theoretical modeling of lipid diffusion in a SLB. (a) Schematic sketch of the model for a SLB with incorporated lipid probes (red lipids). The lipid bilayer is suspended above a solid support at height H and with interleaflet drag coefficient $b_{leaflet}$. η_f^+ and η_f^- are the super- and sub-fluid viscosities, respectively, and η is the surface viscosity associated with each monolayer. For this specific geometry, the terms in Eq. (6) associated with traction on the leaflets from the surrounding fluids are $K^+(q) = -\eta_f^+ q$ and $K^-(q) = -\eta_f^- q \coth(qH) \approx -\eta_f^-/H = -b_{substrate}$. (b) Each diffuser in the RS scheme is represented by a collection of "blobs" packed in concentric circles to fill a disk of radius R. Solid body motion is imposed on the blobs. In our calculations, each disc is composed from hundreds of such blobs.

H is small and the viscosity of the fluid between the membrane and the support is large. (This assumption is validated by the fits to the experiment discussed below.) In this limit, $K^-(q) = -\eta_f^-/H = -b_{substrate}$, which means the lower leaflet is subjected to a simple drag by the underlying support.

With the hydrodynamic model defined, we use the RS scheme[65,66] to calculate the diffusion coefficients of the labeled lipids in each leaflet. We define the regularized Green's function

$$\boldsymbol{T}(\boldsymbol{r};\epsilon) = \int d\boldsymbol{r}' \boldsymbol{T}(\boldsymbol{r}-\boldsymbol{r}')\,\phi_\epsilon(\boldsymbol{r}'), \tag{9}$$

where $\phi_\epsilon(\boldsymbol{r}) = \frac{1}{2\pi\epsilon^2} e^{-\frac{r^2}{2\epsilon^2}}$ is a Gaussian blob function. A force density distributed over the blob envelope $\boldsymbol{f}(r) = \boldsymbol{g}\phi_\varepsilon(\boldsymbol{r})$ will result in a velocity response $v_i^\alpha(\boldsymbol{r}) = T_{ij}^{\alpha\beta}(\boldsymbol{r};\varepsilon)\, g_j^\beta$ [Eq. (4)].

We represent the labeled lipids by a disc centered at the origin and composed of N blobs centered at positions $\{\boldsymbol{R}_n\}$ [see Fig. 5(b)]. The force on blob n is written $\boldsymbol{g}^\alpha[\boldsymbol{R}_n]$ and the fluid response to all such forces [Eq. (4)] predicts the velocity at each $\boldsymbol{R}_m$ which yields the $2N \times 2N$ matrix equation

$$v_i^\alpha[\boldsymbol{R}_m] = \sum_{n=1}^{N} T_{ij}^{\alpha\beta}(\boldsymbol{R}_m - \boldsymbol{R}_n;\epsilon)\, g_j^\beta[\boldsymbol{R}_n]. \tag{10}$$

We chose all blob velocities $\{v[\boldsymbol{R}_n]\}$ to be identical, corresponding to a rigid body translation of the disc in the $\hat{x}$ direction with velocity $\boldsymbol{V} = V\hat{x}$. Equation (10) is numerically solved to obtain the forces $\{g[\boldsymbol{R}_n]\}$ (for a detailed numerical method we refer the reader to Ref. 44) and the total force on the disc follows as $F = \sum_{n=1}^{N} g[R_n]$. The diffusion coefficient is then obtained from the Einstein relation

$$D = \mu k_b T = \left(\frac{V}{F}\right) k_b T. \tag{11}$$

Fitting procedure

We repeat the RS calculations for various inter-blob spacings s, and define ϵ to be half this spacing. As s decreases, the spatial resolution of the calculation increases. The mobility values were found to change approximately linearly with s[44] thus allowing us to extrapolate to the infinite resolution limit $s \to 0$; these extrapolated values are used to calculate the diffusion coefficients. While using thousands of blobs to construct each diffusing molecule is expected to produce diffusion coefficients with a maximal error of 0.4%,[44] the calculation is time-consuming and cumbersome when used in a numerical fitting procedure (as discussed below), where the mobilities need to be evaluated thousands of times. Limiting the number of blobs to several hundred at the highest resolution and then performing the linear extrapolation produces results with maximal error of 2%, which is sufficient for our purposes and keeps the fitting procedure practical. (In practice, the results were obtained at four different resolutions: 106, 252, 440, and 534 blobs.) During the fitting procedure, we set the membrane viscosity η such that $l_{sd} = \eta/\eta_f = 160$ nm.[69] The viscosity of the water layer above the membrane was set to bulk water viscosity: $\eta_f^+ = 1$ cP[70] and we set the labeled lipid radius $r = 0.5$ nm which is reasonable when taking an area per lipid molecule of $A \approx 0.43$ nm^2 ($r \approx 0.37$ nm) for DMPE[71] and allowing for a hydrodynamic radius slightly larger than the thermodynamic radius due to interactions between lipids.[62] A global fitting algorithm was used to determine values for $b_{leaflet}$ and $b_{substrate}$ that minimize the error between the experimental diffusion coefficients and the coefficients obtained from the RS method, $(D_{fast}^{exp} - D_{fast}^{RS})^2 + (D_{slow}^{exp} - D_{slow}^{RS})^2$. As Atto647N-DMPE shows significantly different flip-flop rates between the upper and lower leaflets depending upon the flip direction, potentially indicating some manner of dye-substrate interaction, while Atto550-DMPE reveals better balanced rates (see Table S1 of the supplementary material) and faster diffusion, we have fit only to the diffusion coefficients of the latter. The best fit parameters are presented in Table II for both membrane types.

TABLE II. Results of the RS fitting procedure. Diffusion coefficients (D_{fast}, D_{slow}) reproduce the experimental values. The drag coefficients ($b_{leaflet}$, $b_{substrate}$) were extracted from the fitting procedure assuming the listed values for η_f^+, r, and l_{sd}.

	D_{fast} (μm^2/s)	D_{slow} (μm^2/s)	$b_{leaflet}$ (Pa s/m)	$b_{substrate}$ (Pa s/m)
EPC (RT)	4.22	0.079	$2.1 \cdot 10^7$	$1.66 \cdot 10^{10}$
DOPC (RT)	4.89	0.091	$1.07 \cdot 10^7$	$1.44 \cdot 10^{10}$

DISCUSSION

Lipid diffusion in SLBs

In this work, we analyzed the motion of lipid molecules within supported bilayers in the fluid phase. We identified two populations, slow and fast, with well-separated diffusion coefficients, using two different lipid types and two different probes. As noted in the Introduction, bimodal diffusivity has been observed previously in SLBs, yet its source has remained poorly understood. Here we demonstrated that the slow and fast diffusing populations of lipids in SLBs are related to leaflet dynamics, using iodine quenching of fluorescence combined with SPT.

Various ensemble-based methods have been applied to measure differences in the dynamics of the two leaflets of a SLB. Some authors used fluorescence quenching, as in this work, as a means to differentiate between the two leaflets.[19,21] Another approach relied on asymmetric bilayer preparation,[14,19,24] i.e., the incorporation of probes into one of the leaflets. However, this approach can lead to meaningful results only if the bilayer does not equalize its leaflet compositions within the experimental preparation times. Further, it has been suggested that whether or not heterogeneous diffusion is observed does not solely depend on the substrate type and SLB preparation technique,[12,24] but also on the lipid probe used. Indeed, for the same bilayer preparation, either two-component diffusion or one-component diffusion has been observed, depending on the lipid probe.[11,21] Instructive in this context is the observation that certain probes distribute highly asymmetrically between the two leaflets.[14,21,72] This may lead to the observation of an effective one-component diffusion. (We note that in previous work from our lab,[3] we observed a single diffusion coefficient using lissamine rhodamine B as a label, which might be asymmetrically distributed.) Another problem of ensemble-based measurements such as fluorescence recovery after photobleaching is that high flip-flop rates might average the two diffusion modes into a single apparent mode, especially when the measurement is done over large areas.[25] Indeed, given a diffusion coefficient of $D_{fast} \approx 4\ \mu m^2/s$ of a probe in the upper leaflet and a flip-flop half time $t_{1/2,fast} \approx 5$ s, we calculate that such a probe diffuses only $\langle \Delta r \rangle \approx 9\ \mu m$ before flipping to the lower leaflet. We also note that FCS is not optimal for measuring diffusion coefficients as slow as revealed in our study.[73,74] Importantly, the measurements reported in this paper *do not* depend on asymmetric bilayer preparation nor do they depend on probe distribution. Indeed, in our experiments, the two subpopulations of diffusing lipids are *separately observed and analyzed*. SPT is clearly superior in that respect to ensemble-based methods.

RS hydrodynamic calculations

We have estimated the physical parameters, $b_{substrate}$ and $b_{leaflet}$, governing bimodal diffusion due to different leaflet dynamics using a generalized RS method.[44] Previously, in diffusional studies, the Evans and Sackmann model[28] was used to either estimate properties of the lubricating interfacial layer,[12,18] i.e., the interfacial drag coefficient $b_{substrate}$, or the inter-monolayer friction coefficient $b_{leaflet}$ inherent to the bilayer structure.[18,29] The former approach relies on the approximation that $b_{leaflet} \gg b_{substrate}$, and thus the membrane acts as a single sheet, whereas the latter approach assumes that $b_{substrate} \gg b_{leaflet}$, with the upper leaflet sliding over a nearly fixed lower leaflet. Nano-rheological approaches and approaches relying on external shear forces to quantify SLB friction suffer from similar considerations.[75,76] Here we have modeled the bilayer nature of a SLB based on a RS scheme that includes both substrate drag via $b_{substrate}$ as well as inter-leaflet drag via $b_{leaflet}$, without imposing assumptions on the relative strength of these parameters. The interleaflet drag $b_{leaflet} \approx 1 \cdot 10^7$ Pa s/m we find is in agreement with other measurements obtained for SLBs (i.e., $1 \cdot 10^7$–$1 \cdot 10^8$ Pa s/m).[18,29,75] However, our calculations suggest that the viscosity of the confined interfacial water in the subfluid is elevated by $\sim 10^4$ as compared to bulk water. Assuming the membrane distance from the support at a constant value of $H = 0.7$ nm (which is within the range of values reported for supported membranes $H \approx 0.5$–3 nm),[72,77–81] and using[28] $b_{substrate} \approx \eta_f^-/H$ we obtain $\eta_f^- \approx 10$ Pa s (bulk water has $\eta_f^+ \approx 0.001$ Pa s). Other approaches to measure $b_{substrate}$ are limited by assuming weak substrate coupling and thus not surprisingly reveal lower coupling.[12,18,76] It is likely that the surface treatment before SLB preparation affects the properties of the water layer under the SLB, for example, by changing the apparent viscosity of the nanoconfined water, as was shown for solid surfaces with different wettabilities by measuring shear viscous forces with an AFM tip.[82] Though the value of the effective viscosity of nanometer scale interfacial water remains controversial,[83] values $\sim 10^2$-10^6 times greater than bulk water have previously been measured for hydrophilic substrates,[82,84] indicating that the present measurement may be reasonable. Another possibility however is that $b_{substrate}$ inferred through the comparison between experiment and modeling in this work may not originate from simple hydrodynamic considerations. The modeling (in the parameter regime relevant to the experiments) is only sensitive to a friction coefficient of some origin and cannot distinguish whether the underlying cause of this drag is a high fluid viscosity in the trapped water region or reflects some other mechanism of dissipation.

Lipid flip-flop in SLBs

We observed transitions between slow and fast diffusion in some of our single-molecule trajectories and assigned them to flip-flop of lipids between the two membrane leaflets. Flip-flop half times, $t_{1/2}$, in the range of hours to days were reported for unilamellar vesicles.[35,85] In contrast, the transbilayer motion is faster by orders of magnitudes in SLBs, with measured half-times in the range of minutes[30] or even faster.[31–34] In this work, we found that the flip-flop half-times are indeed in the range of seconds. We would like to emphasize that single molecule analysis with high temporal resolution is essential in determining these short flip-flop half times, whereas many ensemble-based approaches lack the temporal resolution necessary to measure sub-minute half times.[30–33] Interestingly, our values are 2-3 orders of magnitude shorter than the half times in ensemble experiments on a similar system of Atto633-DOPE in DOPC/DOPS SLBs.[30] It is possible that labeling

of the lipids alters the free energy barrier for flip-flop, and indeed label-induced alterations in lipid flip-flop rates have been proposed in the literature.[32,85–87] However, label-free measurements[31–34] also suggested very fast flip-flop dynamics, which seem to agree, at least qualitatively, with our results. The similarity of these results to ours suggests that hydrophobic or membrane interacting dyes,[61] as used in our study, do not perturb the flip-flop process.

Lipid flip-flop dynamics in free standing membranes are considered to be mediated by transient structural defects that lower the resistance for the polar lipid head groups to pass the hydrophobic membrane core.[63] It has been speculated that enhanced flip-flop rates in SLBs are due to similar defects.[35] By contrast, in a recent study, it was proposed that in defect free SLBs, fast flip-flop is driven by surface induced disorder of the bilayer's acyl chain packing.[33] Indeed, it has been shown that in the fluid phase, sufficiently above the main transition temperature, vesicle-deposited SLBs form continuous and largely defect-free bilayers.[9,10,13,88] Our analysis allowed us to directly test the involvement of defects in the flip-flop reactions in a SLB. We find that at RT, transbilayer transitions are not clustered in specific points on the surface but are rather randomly distributed, consistent with a flip-flop mechanism that does not involve defects. At a lower temperature, it seems that membrane defects play some role in enhancing the flip-flop rates. The transition temperature (T_m) of DOPC[89] is −16.5 °C and thus the SLB is supposed to remain sufficiently far from its main liquid-to-solid transition at 10 °C, although the transition broadens considerably due to the presence of a support.[13] It is therefore likely that the cooling of the sample itself creates defects due to a reduction in the area per molecule[90] of the DOPC lipids in the bilayer.

CONCLUSION

In this work, we presented a detailed analysis of lipid diffusion in SLBs. We found two well-separated populations of slow and fast diffusing lipids that we can associate with the lower and upper leaflet, respectively. While labeling effects are of some concern in deducing self-contained lipid behavior, the direct observation of lipid subpopulations clearly demonstrates the benefits of SPT over ensemble-based approaches. Unlocking the immanent dynamics of each population, we could also characterize the flip-flop kinetics of the lipids, which were found to occur on a time scale of seconds. We have further supported our measurements with hydrodynamic calculations that revealed the physical parameters governing bimodal diffusion due to the bilayer structure of SLBs and showed that the viscosity of the water layer trapped under the SLB is $\sim 10^4$ larger than the viscosity of free water. The complex and rich picture emerging from these studies reveals the various influences of the support on lipid behavior and dynamics in the two distinct leaflets of a supported membrane.

SUPPLEMENTARY MATERIAL

See supplementary material for detailed description of the experimental setup and methods used for particle tracking and data analysis.

ACKNOWLEDGMENTS

We thank Dr. Haim Aviram for providing protein L and for his help with building the microscopy setup. We further thank Dr. Menahem Pirchi for contributing code for the HMM analysis, and Professor Haim Diamant for many discussions. This work was supported by Grant No. 2012084 from the U.S.-Israel Binational Science Foundation, and in part by Grant No. CHE-1465162 from the National Science Foundation of the United States. R.L.S. was supported by a post-doctoral fellowship from the Swiss National Science Foundation (SNSF).

[1] C. M. Rosetti, A. Mangiarotti, and N. Wilke, Biochim. Biophys. Acta, Biomembr. **1859**, 789 (2017).
[2] G. J. Hardy, R. Nayak, and S. Zauscher, Curr. Opin. Colloid Interface Sci. **18**, 448 (2013).
[3] M. Ott, Y. Shai, and G. Haran, J. Phys. Chem. B **117**, 13308 (2013).
[4] R. Macháň and M. Hof, Biochim. Biophys. Acta, Biomembr. **1798**, 1377 (2010).
[5] P. Cheney, A. Weisgerber, A. Feuerbach, and M. Knowles, Membranes **7**, 15 (2017).
[6] D. W. Lee, H.-L. Hsu, K. B. Bacon, and S. Daniel, PLoS One **11**, e0163437 (2016).
[7] S.-T. Yang, V. Kiessling, J. A. Simmons, J. M. White, and L. K. Tamm, Nat. Chem. Biol. **11**, 424 (2015).
[8] D. Keller, N. B. Larsen, I.M. Møller, and O. G. Mouritsen, Phys. Rev. Lett. **94**, 025701 (2005).
[9] Z. V. Feng, T. A. Spurlin, and A. A. Gewirth, Biophys. J. **88**, 2154 (2005).
[10] A. Charrier and F. Thibaudau, Biophys. J. **89**, 1094 (2005).
[11] A. R. Burns, D. J. Frankel, and T. Buranda, Biophys. J. **89**, 1081 (2005).
[12] K. J. Seu, A. P. Pandey, F. Haque, E. A. Proctor, A. E. Ribbe, and J. S. Hovis, Biophys. J. **92**, 2445 (2007).
[13] S. Garcia-Manyes, G. Oncins, and F. Sanz, Biophys. J. **89**, 4261 (2005).
[14] J. M. Crane, V. Kiessling, and L. K. Tamm, Langmuir **21**, 1377 (2005).
[15] S. Chiantia, J. Ries, N. Kahya, and P. Schwille, ChemPhysChem **7**, 2409 (2006).
[16] M. Przybylo, J. Sýkora, J. Humpolíčková, A. Benda, A. Zan, and M. Hof, Langmuir **22**, 9096 (2006).
[17] A. Sharonov, R. Bandichhor, K. Burgess, A. D. Petrescu, F. Schroeder, A. B. Kier, and R. M. Hochstrasser, Langmuir **24**, 844 (2008).
[18] R. Merkel, E. Sackmann, and E. Evans, J. Phys. **50**, 1535 (1989).
[19] L. Zhang and S. Granick, J. Chem. Phys. **123**, 211104 (2005).
[20] A. Benda, M. Beneš, V. Mareček, A. Lhotský, W. T. Hermens, and M. Hof, Langmuir **19**, 4120 (2003).
[21] P. Jönsson, J. P. Beech, J. O. Tegenfeldt, and F. Höök, J. Am. Chem. Soc. **131**, 5294 (2009).
[22] M. Hetzer, S. Heinz, S. Grage, and T. M. Bayerl, Langmuir **14**, 982 (1998).
[23] A. Matysik and R. S. Kraut, J. Visualized Exp. **88**, e52054 (2014).
[24] C. Scomparin, S. Lecuyer, M. Ferreira, T. Charitat, and B. Tinland, Eur. Phys. J. E **28**, 211 (2009).
[25] G. J. Schütz, H. Schindler, and T. Schmidt, Biophys. J. **73**, 1073 (1997).
[26] T. E. Starr and N. L. Thompson, Langmuir **16**, 10301 (2000).
[27] T. Dertinger, I. von der Hocht, A. Benda, M. Hof, and J. Enderlein, Langmuir **22**, 9339 (2006).
[28] E. Evans and E. Sackmann, J. Fluid Mech. **194**, 553 (1988).
[29] S. R. Tabaei, J. J. J. Gillissen, and N.-J. Cho, Small **12**, 6338 (2016).
[30] A. Kułakowska, P. Jurkiewicz, J. Sýkora, A. Benda, Y. Mely, and M. Hof, J. Fluoresc. **20**, 563 (2010).
[31] Y. Gerelli, L. Porcar, L. Lombardi, and G. Fragneto, Langmuir **29**, 12762 (2013).
[32] J. Liu and J. C. Conboy, Biophys. J. **89**, 2522 (2005).
[33] B. Wah, J. M. Breidigan, J. Adams, P. Horbal, S. Garg, L. Porcar, and U. Perez-Salas, Langmuir **33**, 3384 (2017).
[34] T. C. Anglin and J. C. Conboy, Biochemistry **48**, 10220 (2009).
[35] D. Marquardt, F. A. Heberle, T. Miti, B. Eicher, E. London, J. Katsaras, and G. Pabst, Langmuir **33**, 3731 (2017).
[36] A. O. Barden, A. S. Goler, S. C. Humphreys, S. Tabatabaei, M. Lochner, M. Ruepp, T. Jack, J. Simonin, A. J. Thompson, J. P. Jones, and J. A. Brozik, Neuropharmacology **98**, 22 (2015).
[37] M. J. Saxton, *Fundamental Concepts in Biophysics* (Humana Press, Totowa, NJ, 2009), pp. 1–33.

[38]H. Shen, L. J. Tauzin, R. Baiyasi, W. Wang, N. Moringo, B. Shuang, and C. F. Landes, Chem. Rev. **117**, 7331 (2017).
[39]S. T. Low-Nam, K. A. Lidke, P. J. Cutler, R. C. Roovers, P. M. P. van Bergen en Henegouwen, B. S. Wilson, and D. S. Lidke, Nat. Struct. Mol. Biol. **18**, 1244 (2011).
[40]A. Sergé, N. Bertaux, H. Rigneault, and D. Marguet, Nat. Methods **5**, 687 (2008).
[41]C. Manzo and M. F. Garcia-Parajo, Rep. Prog. Phys. **78**, 124601 (2015).
[42]N. Komura, K. G. N. Suzuki, H. Ando, M. Konishi, M. Koikeda, A. Imamura, R. Chadda, T. K. Fujiwara, H. Tsuboi, R. Sheng, W. Cho, K. Furukawa, K. Furukawa, Y. Yamauchi, H. Ishida, A. Kusumi, and M. Kiso, Nat. Chem. Biol. **12**, 402 (2016).
[43]L. R. Rabiner, Proc. IEEE **77**, 257 (1989).
[44]B. A. Camley and F. L. H. Brown, Soft Matter **9**, 4767 (2013).
[45]E. Boukobza, A. Sonnenfeld, and G. Haran, J. Phys. Chem. B **105**, 12165 (2001).
[46]J.-C. Olivo-Marin, Pattern Recognit. **35**, 1989 (2002).
[47]K. I. Mortensen, L. S. Churchman, J. A. Spudich, and H. Flyvbjerg, Nat. Methods **7**, 377 (2010).
[48]T. A. Laurence and B. A. Chromy, Nat. Methods **7**, 338 (2010).
[49]K. Jaqaman, D. Loerke, M. Mettlen, H. Kuwata, S. Grinstein, S. L. Schmid, and G. Danuser, Nat. Methods **5**, 695 (2008).
[50]C. L. Vestergaard, Phys. Rev. E **94**, 022401 (2016).
[51]H. Deschout, K. Neyts, and K. Braeckmans, J. Biophotonics **5**, 97 (2012).
[52]X. Michalet, Phys. Rev. E **82**, 041914 (2010).
[53]J. Schuster, F. Cichos, and C. von Borczyskowski, J. Phys. Chem. A **106**, 5403 (2002).
[54]F.-X. Contreras, A. M. Ernst, F. Wieland, and B. Brugger, Cold Spring Harbor Perspect. Biol. **3**, a004705 (2011).
[55]T. Heimburg, B. Angerstein, and D. Marsh, Biophys. J. **76**, 2575 (1999).
[56]I. Levental and S. L. Veatch, J. Mol. Biol. **428**, 4749 (2016).
[57]E. Sezgin, I. Levental, S. Mayor, and C. Eggeling, Nat. Rev. Mol. Cell Biol. **18**, 361 (2017).
[58]D. B. Chalpin and A. M. Kleinfeld, Biochim. Biophys. Acta, Biomembr. **731**, 465 (1983).
[59]Y. Barenholz, T. Cohen, R. Korenstein, and M. Ottolenghi, Biophys. J. **60**, 110 (1991).
[60]A. Chmyrov, T. Sandevn, and J. Widengren, J. Phys. Chem. B **114**, 11282 (2010).
[61]L. D. Hughes, R. J. Rawle, S. G. Boxer, S. Doose, and M. Heilemann, PLoS One **9**, e87649 (2014).
[62]M. J. Skaug, M. L. Longo, and R. Faller, J. Phys. Chem. B **113**, 8758 (2009).
[63]F.-X. Contreras, L. Sánchez-Magraner, A. Alonso, and F. M. Goñi, FEBS Lett. **584**, 1779 (2010).
[64]P. M. Dixon, *Encyclopedia of Environmetrics* (John Wiley & Sons, Ltd., Chichester, UK, 2006).
[65]R. Cortez, L. Fauci, and A. Medovikov, Phys. Fluids **17**, 31504 (2005).
[66]R. Cortez, SIAM J. Sci. Comput. **23**, 1204 (2001).
[67]U. Seifert and S. A. Langer, Europhys. Lett. **23**, 71 (1993).
[68]F. L. H. Brown, Q. Rev. Biophys. **44**, 391 (2011).
[69]S. Ramadurai, A. Holt, V. Krasnikov, G. van den Bogaart, J. A. Killian, and B. Poolman, J. Am. Chem. Soc. **131**, 12650 (2009).
[70]W. M. Haynes, D. R. Lide, and T. J. Bruno, *CRC Handbook of Chemistry and Physics: A Ready-Reference Book of Chemical and Physical Data* (CRC Press, 2013).
[71]K. Graf and H. Riegler, Colloids Surf., A **131**, 215 (1998).
[72]C. M. Ajo-Franklin, C. Yoshina-Ishii, and S. G. Boxer, Langmuir **21**, 4976 (2005).
[73]M. Rose, N. Hirmiz, J. Moran-Mirabal, and C. Fradin, Membranes **5**, 702 (2015).
[74]J. Ries and P. Schwille, Phys. Chem. Chem. Phys. **10**, 3487 (2008).
[75]P. Jönsson, J. P. Beech, J. O. Tegenfeldt, and F. Höök, Langmuir **25**, 6279 (2009).
[76]S. Leroy, A. Steinberger, C. Cottin-Bizonne, A.-M. Trunfio-Sfarghiu, and E. Charlaix, Soft Matter **5**, 4997 (2009).
[77]B. W. Koenig, S. Krueger, W. J. Orts, C. F. Majkrzak, N. F. Berk, J. V Silverton, and K. Gawrisch, Langmuir **12**, 1343 (1996).
[78]V. Kiessling and L. K. Tamm, Biophys. J. **84**, 408 (2003).
[79]A. R. Ferhan, J. A. Jackman, and N.-J. Cho, Anal. Chem. **89**, 4301 (2017).
[80]S. J. Johnson, T. M. Bayerl, D. C. McDermott, G. W. Adam, A. R. Rennie, R. K. Thomas, and E. Sackmann, Biophys. J. **59**, 289 (1991).
[81]D. A. Doshi, A. M. Dattelbaum, E. B. Watkins, C. J. Brinker, B. I. Swanson, A. P. Shreve, A. N. Parikh, and J. Majewski, Langmuir **21**, 2865 (2005).
[82]D. Ortiz-Young, H.-C. Chiu, S. Kim, K. Voïtchovsky, and E. Riedo, Nat. Commun. **4**, 2482 (2013).
[83]U. Raviv, P. Laurat, and J. Klein, Nature **413**, 51 (2001).
[84]M. P. Goertz, J. E. Houston, and X.-Y. Zhu, Langmuir **23**, 5491 (2007).
[85]M. Nakano, M. Fukuda, T. Kudo, N. Matsuzaki, T. Azuma, K. Sekine, H. Endo, and T. Handa, J. Phys. Chem. B **113**, 6745 (2009).
[86]I. López-Montero, N. Rodriguez, S. Cribier, A. Pohl, M. Vélez, and P. F. Devaux, J. Biol. Chem. **280**, 25811 (2005).
[87]S. Garg, L. Porcar, A. C. Woodka, P. D. Butler, and U. Perez-Salas, Biophys. J. **101**, 370 (2011).
[88]R. Richter, A. Mukhopadhyay, and A. Brisson, Biophys. J. **85**, 3035 (2003).
[89]A. S. Ulrich, M. Sami, and A. Watts, Biochim. Biophys. Acta, Biomembr. **1191**, 225 (1994).
[90]J. Pan, S. Tristram-Nagle, N. Kučerka, and J. F. Nagle, Biophys. J. **94**, 117 (2008).